 doi:10.20944/preprints202011.0226.v1

Article

ACTIVATED CARBON FROM WINEMAKING WASTE: THERMOECONOMIC ANALYSIS FOR LARGE-SCALE PRODUCTION

Isaac Lorero[1], Arturo Javier Vizcaíno[2], Francisco J. Alguacil[3] and Félix A. López[3]

[1] Materials Science and Engineering Area, Rey Juan Carlos University, C/Tulipán s/n, Móstoles, 28933, Madrid, Spain; isaac.lorero@urjc.es (I.L.)
[2] Chemical and Environmental Engineering Group, Rey Juan Carlos University, C/ Tulipán, s/n, Móstoles 28933, Spain; arturo.vizcaino@urjc.es (A.J.V.)
[3] National Center for Metallurgical Research (CENIM). Spanish National Research Council (CSIC). Avda. Gregorio del Amo, 8. 28040, Madrid, Spain; fjalgua@cenim.csic.es (F.J.A.)

* Correspondence: f.lopez@csic.es ; Tel.: +34-9155 -38900 (F.A.L.)

Abstract:

An activated carbon manufacturing process using winemaking waste is analyzed and designed at industrial scale. Starting from experimental research, the chemical transformations and thermodynamics during pruning wood conversion are studied as a basis for plant design. In this way, mass and energy balances of hydrothermal carbonization and physical activation are fulfilled and a thermoeconomic methodology is applied to develop an energy-integrated plant. To achieve this target, a network of heat exchangers is allocated to minimize heat consumption and supply hot domestic water, while a cogeneration cycle is designed to provide electricity and satisfy the remaining heat demand. Furthermore, a sensitivity analysis is carried out to determine the influence of the production scale and other operation parameters, such as annual workload, service life, and capital and feedstock costs, on the economic viability of the plant. The energy balance of the plant indicates that the energy integration design manages to provide 48.9% of the overall process energy demand by crossing hot and cold streams and recovering heat from residual flue gas. On the other hand, the exergy cost analysis identifies the combustion of pruning wood used to provide heat demands as the main source of exergy destruction, confirming the suitability of integration to improve the thermodynamic performance. Including activated carbon production, electricity, and hot domestic water, the exergy efficiency of the plant stands at 11.5%.

Keywords: activated carbon; hydrothermal carbonization (HTC); exergy analysis; thermoeconomic analysis; circular economy.

1. Introduction

Concepts related to sustainable development stand out among the most influential topics at present, such as replacement of non-renewable resources, reduction of wastes and greenhouse emissions, and the improvement of energy efficiency. In this regard, the European Union launched its political strategy in 2015 to impulse its socioeconomic transition to a new model through the document "Closing the loop: An EU action plan for the Circular Economy" [1]. The plan includes several investments to encourage innovative and efficient companies and is considered by the Brussels authorities to provide the opportunity to reinvent the European economy and keep it in vanguard [2]. Looking at its economic activity, the agri-food industry appears as a chance to research new processes to make consumer goods from its wastes. The wine industry, which generates an abundant amount of organic wastes, such as vine shoots and grape marc and seeds, is an appropriate example. The Spanish wine sector has a strong presence in global production, with an

 doi:10.20944/preprints202011.0226.v1

average grape demand that oscillates between five and seven million tons every year. However, approximately 17% of this net weight ends up as waste. The relatively ease and mass availability, adequate properties, and low price of these organic residues make it an interesting resource from which to obtain biochar and activated carbon [3].

There currently exist many different thermal treatments to obtain char from biomass [4–10]. One of them is hydrothermal carbonization (HTC), which consists of the coalification of organic materials under an inert atmosphere, suspended inside an aqueous phase at sub-critical conditions. This process is performed by applying high temperatures (usually between 180 ºC and 250 ºC) and pressures (above the saturation pressure, generally from 10 to 50 bar) over a huge range of times (from a few minutes to several hours) [11–15]. These conditions change the chemical properties of water and make it an adequate solvent for biomass coalification treatments. The hydrothermal reaction of lignocellulosic materials begins when the temperature rises to 180 ºC and the hydrolysis of hemicellulose starts. Hydrolysis of cellulose and decomposition of lignin occur when temperatures ascend to 230 ºC and 250 ºC, respectively [13].

Dehydration and decarboxylation of oligomers generate a series of organic acids, phenolic products, and furan derivates. Part of these products continue its decomposition and form a gaseous phase composed basically of CO_2 and minor quantities of CO, CH_4, and H_2. The range of products and quantities depend on the specific conditions of the process. At lower temperatures and pressures, biomass decomposition tends to moderate rates and solid yield predominates. As the treatment becomes more aggressive (i.e., with higher temperatures and pressures or with the addition of organic solvents), liquid and gas formation is favored [11–13],[15–18]. Hydrothermal cracking increases the carbon content and calorific power of treated solids, making them interesting energy alternatives to fossil fuels [18,19]. Hydrochar also presents good properties as a precursor for activated carbons [20,21], expanding its range of applications to different uses such as pollutant removal [22,23], hydrogen storage [24], batteries and supercapacitors [25,26], or additives for livestock feed [27].

Activated carbons are obtained by treating carbonaceous sources with activating agents, which deeply increase its surface area. Depending on the substances used during activation, two different routes can be distinguished. In the chemical route, the precursor is mixed with a chemical reagent—usually KOH [20],[22], $ZnCl_2$ [23], or H_3PO_4 [28]—which provokes oxidation and swelling under inert atmospheres at temperatures between 200 and 1000 ºC. On the other hand, in the physical approach, the carbonaceous solid reacts with an oxidizing gas—usually steam or CO_2—at temperatures between 700 and 1000 ºC [20], [22],[29].

Although chemical routes usually confer larger surface areas and better adsorption capabilities to the activated carbons, compared with physical routes [20],[22],[30], their industrial competitiveness is lacking, due to the greater costs and complexity [31].

Interest in the research and production of hydrothermal carbon from biomass and wastes has grown over the past decade. Some publications have analyzed the feasibility of these methods [13,14],[32–35] and a few pilot plants have even been built and put into operation [36]. In this regard, exergy and thermoeconomic analyses are useful tools to optimize the process, which have barely been employed in hydrochar and activated carbon processes. By applying thermodynamic principles, these studies provide suitable information to identify energy and economic process inefficiencies. Through a comprehensive assessment, opportune improvements can be defined and applied to the examined plants [37,38]. As examples of these reports, we cite the biomass gasification system developed by Yang et al. [39], the Organic Rankine Cycle and Vapor Compression Cycle hybrid system analyzed by Karellas and Braimakis [40], or the technoeconomic review of hydrothermal oxidation of food waste for hydrochar and bio-oil production made by Mahmood et al. [41].

Following this trend, the present work tackles the design and thermoeconomic analysis of an industrial-scale continuous plant for activated carbon production using vineyard pruning wood. To achieve a realistic, sustainable, and eco-friendly process, laboratory research data are used to examine the thermodynamics of hydrothermal carbonization and physical activation reactions, in order to carry out a thorough thermoeconomic analysis. In this way, energy integration of the

Preprints (www.preprints.org) | NOT PEER-REVIEWED | Posted: 6 November 2020 doi:10.20944/preprints202011.0226.v1

process, including a cogeneration system fed by the same wood residues used raw, is proposed and analyzed, in order to foster energy self-sustainable production. Finally, a sensitivity analysis is applied to determine the plant profitability, based on different production and economic scenarios.

2. Materials and Methods

2.1. Experimental data

Vineyard pruning wood was received from the Biological Mission of Galicia (CSIC, northwest Spain) and crushed to a grain size of <2 mm using an SK 100 Cross Beater Mill to increase the surface area and reactivity. Then, the pruning wood was mixed with water (74 grams of solid per liter of water) and introduced into a Berghof BR-100 reactor. The carbonization pressure was set at 50 bar, while different times (1 to 7 hours) and temperatures (150 to 250 ºC) were tested. Supplementary Fig. S1 shows the solid yield of HTC of vineyard pruning wood under the different mentioned experimental conditions, as well as the variation of elemental composition after 1 hour of treatment. The increase of temperature showed a stronger influence, leading to lower solid yields but achieving hydrochar with higher carbon contents; a characteristic that is desirable for the subsequent production of activated carbon. Thus, hydrothermal cracking was established at 250 ºC for 1 hour. Under these conditions, the reaction mass balance is shown in Supplementary Table S1.

Total organic carbon (TOC) of the liquid phase was determined using a combustion/non-dispersive infrared gas analyzer (model TOC-V Shimadzu). Afterwards, the liquid phase was separated into two fractions by evaporation in a rotary evaporator (Buchi Mod. R300), in order to determine its chemical composition.

The condensable phase consisted of an azeotropic mixture of water and minor contents of acetic acid, which were estimated through acid–base titration using a 1 M NaOH solution. On the other hand, the composition of the organic non-condensable phase was determined by gas chromatography-mass spectrometry (GC-MS). Analyzed samples of the non-condensable phase were diluted in dichloromethane at concentrations between 40 and 42 mg/ml and were injected immediately into the chromatograph. This analysis was done with an Agilent 7890A equipped with an Agilent MS5975C mass spectrometer and a 30 m long HP-5ms (5% phenyl-methylpolysiloxane) column. The chemical composition and elemental C, H, and O proportions of this organic phase are noted in Supplementary Tables S2 and S3. In order to make analysis of the process viable, the liquid phase composition was simplified by selecting chemical compounds among those detected in the GC-MS, based on the bibliographic disposability of thermodynamic data [42,43]. Their mass percentages were recalculated to maintain real carbon, hydrogen, and oxygen proportions. Gaseous products could not be determined experimentally, and their compositions were estimated through elemental C, H, and O mass balances, considering other biomass HTC studies published in the literature. As mentioned in the introduction, it is reasonable to expect a gaseous phase composed fundamentally of CO_2 and minor contents of CO, CH_4, and H_2 [11],[16],[32,33]. The formation of other gaseous products was disregarded. Tables S4 and S5 note the estimated mass balance for the vineyard pruning wood hydrothermal carbonization.

Once HTC was completed, 4 g of hydrochar was physically activated in a rotary kiln by using a steam flow of 0.5 ml/min at 900 ºC for 1 h. During activation, an important carbon fraction is removed as CO, giving place to a microporous network (Fig. S2a) that increases the adsorption capacity [44]. Due to high temperatures, a slight coalification of the char was still generated and other gaseous products, such as CO_2, H_2, and H_2O may have formed [45]. Activation burn-off gives a first approach to activation degree and further carbonization (Fig. S2b). Its value was calculated through Eq. 1 and reached 38.88%:

$$\text{Burn-off (\%)} = (w_1-w_2)/w_1 \cdot 100, \quad (1)$$

where w_1 and w_2 are the hydrochar and activated carbon masses, respectively. Activation gas composition was estimated through elemental mass balances, as done with the HTC gas phase. In this

Preprints (www.preprints.org) | NOT PEER-REVIEWED | Posted: 6 November 2020 doi:10.20944/preprints202011.0226.v1

regard, significant condensable phases from hydrochar decomposition were not observed. The activation mass balance is shown in Tables S6 and S7.

2.2. Thermodynamic analysis of hydrothermal carbonization and physical activation

Carbonization and activation heat were theoretically determined through the difference of heats of formation of the products and reagents at their respective reaction temperatures. Except for pruning wood, hydrochar, and activated carbon, all standard enthalpies of formation and specific heat capacities can be found in the bibliography. The heats of formation of these three compounds were estimated through their heats of combustion, which were experimentally measured using a calorimetric bomb. Through modelling a generic combustion reaction (Eq. 2) [16], these enthalpies can be calculated as the difference between the heat of formation of combustion products (CO_2 and H_2O) and the higher heating value (HHV) of solids:

$$CH_xO_y\,(s) + \left(1 + \frac{x}{4} + \frac{y}{2}\right)O_2\,(g) \xrightarrow{HHV} CO_2\,(g) + \left(\frac{x}{2}\right)H_2O\,(l). \qquad (2)$$

To solve the energy balances of carbonization and activation, solid heat capacities must be estimated by applying previous results for wood thermal properties [44,45]:

$$C_p = \frac{2{,}097u+826}{1+u} + \frac{9.92u+2{,}55}{1+u}T + \frac{0.0002}{1+u}T^2 \qquad u < u_{fsp}, \qquad (3)$$

$$C_p = \frac{2{,}062u+555}{1+u} + \frac{5.49u+2.95}{1+u}T + \frac{0.0036}{1+u}T^2 \qquad u \geq u_{fsp}, \qquad (4)$$

where u is the moisture content of the material, u_{fsp} is the fiber saturation point (near to 25%), and T is the temperature. It should be considered that the hydrochar moisture varied from 25% after hydrothermal cracking and filtering to 7.5% after the drying step (see Table 1).

Table 1. Moisture and thermodynamic properties of vineyard pruning wood, hydrochar, and activated carbon.

Solid	Chemical formula	Moisture (%)	HHV (kJ g^{-1})	LHV (kJ g^{-1})	Heat of formation (kJ g^{-1})
Pruning wood	$CH_{1.42}O_{0.62}$	3.01	21.25	20.01	-4.09
Hydrochar	$CH_{1.08}O_{0.23}$	25.00 (1)–7.50 (2)	30.41	29.10	-1.95
Activated carbon	$CH_{0.83}O_{0.20}$	-	29.31	28.16	-2.02

(1) Moisture after hydrothermal cracking and filtering. (2) Moisture after drying.

The energy balance revealed that hydrothermal carbonization is an exothermic process with a heat of reaction of -823 Joules per gram of pruning wood (Fig. 1a). This value fit closely with the experimental measurement of -760 J/g obtained by Funke and Ziegler for wood HTC at 240 ºC [46] and the recent assessment done by Pecchi et al. [47] for cellulose and wood. It is pertinent to mark the importance of executing meticulous elemental mass balances based on experimental measurements, in order to prevent unexpected deviations; for example, simplifying the analysis by supposing a gas phase composed entirely of CO_2 would have led to a 35% overestimation of the carbonization heat in the present research.

Otherwise, the physical activation of hydrochar is an endothermic process (Fig. 1.b) and the heat of reaction stands at 2,396 J/g. The strongly endothermic generation of CO and H_2 from the carbon–steam reaction is barely compensated by CO_2 formation by the decomposition of anhydride and carboxyl groups.

Preprints (www.preprints.org) | NOT PEER-REVIEWED | Posted: 6 November 2020 doi:10.20944/preprints202011.0226.v1

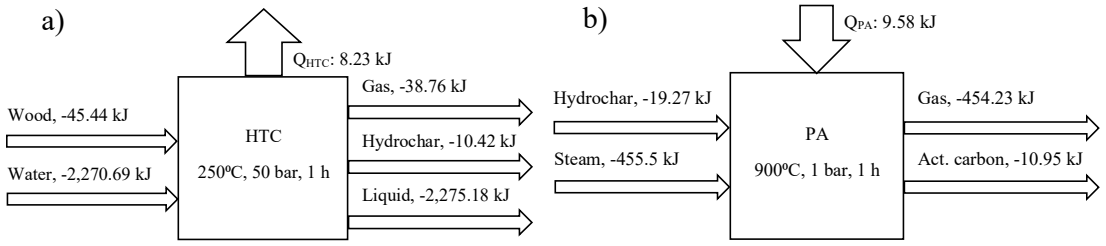

Figure 1. Energy balances per gram of wood of hydrothermal carbonization (a) and physical activation (b).

2.3. System description

Figure 2 shows the industrial-scale continuous process designed for activated carbon production from vineyard pruning wood. This process was established after a previous thermoeconomic study that identified the optimum points for energy integration.

(a)

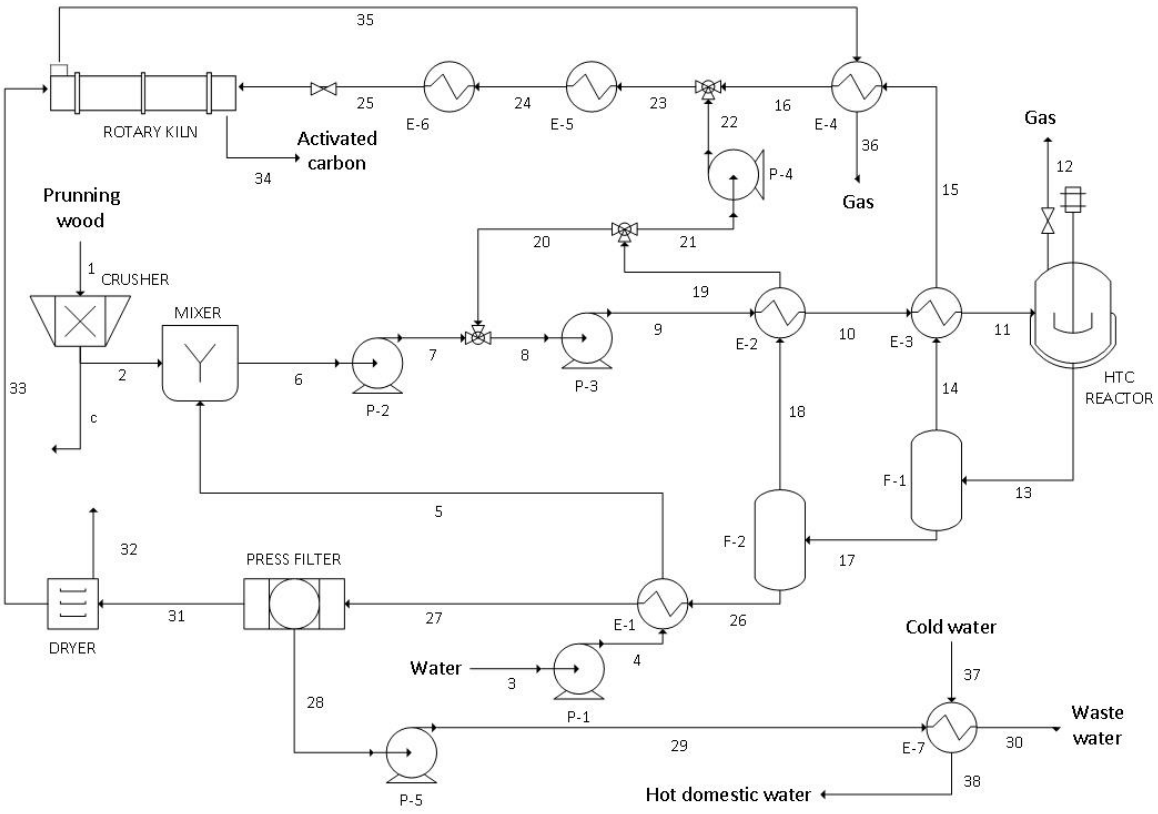

Preprints (www.preprints.org) | NOT PEER-REVIEWED | Posted: 6 November 2020 doi:10.20944/preprints202011.0226.v1

(b)

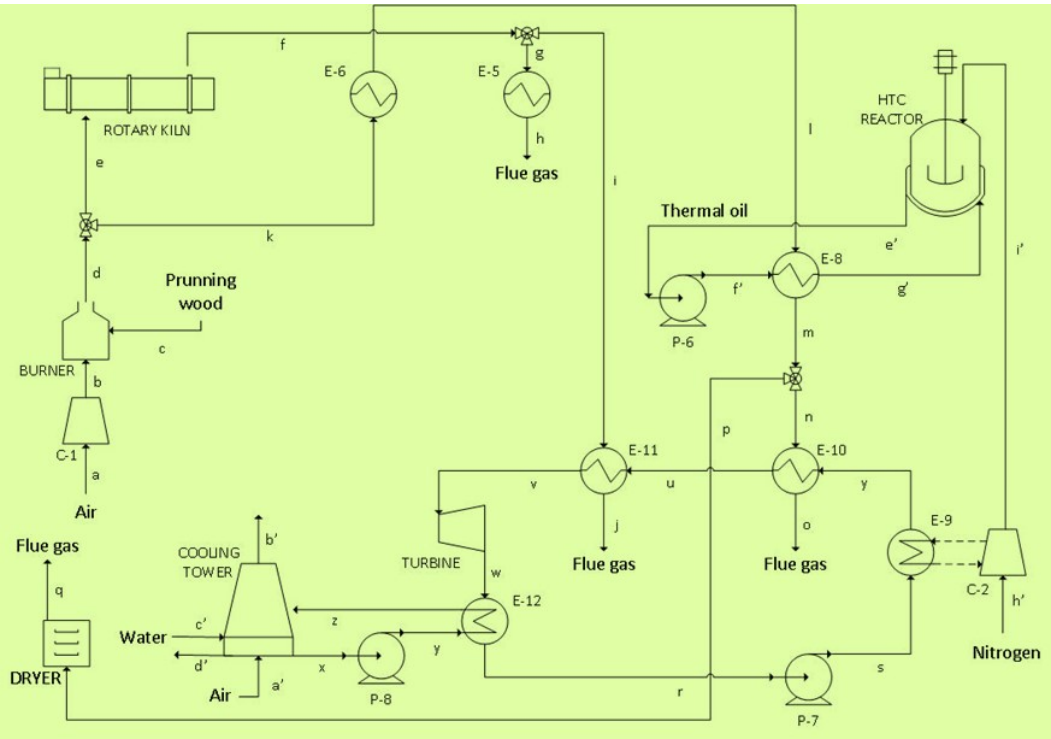

Figure 2. Schematic flow sheet of the activated carbon production plant (a) and the coupled cogeneration system (b).

Vineyard pruning wood is crushed in a crusher to homogenize the particle sizes and increase their surface area and reactivity. Then, part of the wood is mixed with water and pumped into the HTC reactor (Fig. 2a). Simultaneously, compressed nitrogen is introduced into the batch, in order to maintain the pressure at the operation set point (Fig. 2b).

It is worth mentioning that a discontinuous reactor model was selected. Instead of the use of pilot projects with continuous or semi-continuous models, the preference to select current standard equipment and to follow a conservative approach for the cost analysis prevailed. To create a continuous flow, a battery of three batches working in parallel was chosen, in order to avoid the carbonization lapse. The reactors are heated with thermal oil, which takes the heat demand from the flue gas of burned raw material in exchanger E-6.

After HTC reaction, the hydrochar suspension is depressurized to 10 and 3.2 bars in flash tanks F-1 and F-2, respectively. As consequence of both expansions, two steam flows are generated. These flows are used to pre-heat the reactor feed in exchangers E-2 and E-3 and, downstream, as an activating agent into the rotary kiln. Flash pressures are established to warm the HTC inlet below the cellulose hydrolysis point (180 ºC), avoiding fogging in heat exchanger E-3 and premature carbonization. The outgoing slurry from flash tank F-2 is used to pre-heat the inlet water and conduced to a press filter, where the hydrochar is removed from the aqueous phase. This wastewater is pumped to exchanger E-7, in order to transfer its heat and supply a hot domestic water stream. Meanwhile, the char is dried and carried to the rotary kiln to accomplish activation. The activation gas heat is partially recovered in exchanger E-4, in which the condensed flow coming from E-3 is evaporated again.

Otherwise, the part of the crushed pruning wood that is not used to produce activated carbon (stream c) is burned to generate a compressed flue gas, in order to provide the remaining heat demand. To recover the sensible heat of the outgoing flue gas and the excess of heat emitted by the nitrogen compressor C-2, a Rankine cycle is coupled. This steam power cycle works at 60 bar and 480 ºC at the turbine inlet, and generates the electricity necessary for the operation of the entire plant.

Preprints (www.preprints.org) | NOT PEER-REVIEWED | Posted: 6 November 2020 doi:10.20944/preprints202011.0226.v1

2.4. Process thermoeconomic analysis

2.4.1. Incidence matrix

The incidence matrix $A_{(m\,x\,n)}$ represents the physical structure of the process, connecting the m streams and n sub-systems. This matrix ought to be amplified by adding sub-system exergy flows or economic process structure, depending on the thermoeconomic data needed.

To define $A_{(m\,x\,n)}$, each element a_{ij} of the matrix should be valued +1 if stream j enters into sub-system i, -1 if it leaves, or 0 if there does not exist a direct physical connection between them [36]. Under steady-state operation, it is possible to describe mass, energy, and exergy balances using the incidence matrix: A x M = 0, A x E = 0, A x B = B_d, where M, E, B, and B_d are vectors of dimension [n] whose elements correspond to the mass, energy, exergy, and destroyed exergy flows.

2.4.2. Exergy vector

To perform the thermoeconomic analysis, the exergy of each process stream was calculated using the physical (b_p) and chemical (b_c) exergies of the contained substances (Eqs. 5-7):

$$\mathbf{b_p = (H - H^0) - T_0(S - S_0)}, \quad (5)$$

$$\mathbf{b_c = \sum x_i \cdot b_{c,i} + RT_0 \sum x_i \cdot \ln x_i}, \quad (6)$$

$$\mathbf{b - b_p + b_c}. \quad (7)$$

Pruning wood, hydrochar, and activated carbon chemical exergies were estimated using their Lower Heating Values (LHV) in Eq. 7 [48]:

$$\mathbf{b_c = \beta \cdot LHV}, \quad (8)$$

where $\boldsymbol{\beta}$ is a correlation that depends on the chemical composition of the solid [46]:

$$\beta = \frac{1.0412 + 0.216(z_H/z_C) - 0.2499(z_O/z_C)[1 + 0.7884(z_H/z_C)] + 0.045(z_N/z_C)}{1 - 0.3035(z_O/z_C)}, \quad (9)$$

where z_H, z_C, and z_O are the hydrogen, carbon, and oxygen mass fractions of the solids, respectively.

Finally, the exergy vector is completed by adding the exergy flows in each plant device. By multiplying an amplified incidence matrix and the exergy vector, the exergy destruction at each process stage can be determined.

2.4.3. Exergy costs

The exergy cost balance is defined by Equation 10 [36]:

$$\mathbf{B^*_{(n\,x\,1)} = A^{-1}_{(n\,x\,n)} \cdot \Omega_{(n\,x\,1)}}, \quad (10)$$

Preprints (www.preprints.org) | NOT PEER-REVIEWED | Posted: 6 November 2020 doi:10.20944/preprints202011.0226.v1

where B* is the exergy cost vector, $A^{-1}_{(n\,x\,n)}$ is the inverse of the amplified incidence matrix A (m x n)

with economic structure matrix $\alpha_{(n-m)\,x\,n}$, and Ω is the vector of imputed exergy costs. All elements of α are null, except for the following cases:

- Resources: a value of +1 is assigned to the α_{ir} elements corresponding to input resources;
- Products and by-products: a value of +1 is attributed to the α_{ip} elements belonging to process products or by-products;
- Wastes: a value of +1 is assigned to the α_{iw} elements corresponding waste streams; and
- Bifurcations: in those sub-systems with various exiting streams, values of $+1/\dot{B}_j$ and $1/\dot{B}_k$ are assigned to the corresponding *j* and *k* flows.

The vector Ω is defined by a series of null elements that correspond to the *m* rows of the process physical structure, while the other *n-m* elements are established as follows:

- Resources: The values of $\dot{B}_r$, corresponding to resources exergy flows, are imputed; and
- Wastes and bifurcations: null values are assigned.

By solving the exergy cost balance, the rational yield (τ) is obtained. This parameter denotes the process overall efficiency, relating the exergy contained in products with the exergy needed to obtain them:

$$\tau = \frac{\dot{B}_p}{B_p^*}. \quad (11)$$

2.4.4. Economic costs

The economic cost balance is calculated using Eq. 12. It expresses the cost of the outputs through the cost of inputs and fixed costs (e.g., depreciation, maintenance, operations, and general plant expenses):

$$\Pi_{(nx1)} = -A^{-1}_{(nxn)} \cdot \Phi_{(nx1)}. \quad (12)$$

The execution of the economic balance is quite similar to the exergetic cost balance. The same matrix is used, corresponding to imputed thermoeconomic costs. Φ is composed of the m sub-systems and the n-m costs of resources, by-products, wastes, and bifurcations. Otherwise, is the thermoeconomic costs vector, which indicates how expensive the manufactured products are.

The economic balance is based on equipment investments. Equipment prices were estimated by bibliographic procedures [49–51] and actualized according to the Chemical Engineering Price Cost Index [52]. Through this spending (C), the amount of capital needed to create the plant was deduced using the Lang method [53]. Once the plant investment (PI) is estimated, the annualized fixed costs flow (FCA) can be calculated by Eq. 13:

$$FC_A = \left(A/P_{i,n} + f_{RM}\right) \cdot PI, \quad (13)$$

where $A/P_{i,n}$ is the capital recovery factor and f_{RM} is the repair and maintenance factor. The capital recovery factor is determined by cost of capital (i) and plant lifetime (n) in years:

$$A/P_{i,n} = \frac{i \cdot (1+i)^n}{(1+i)^n - 1}, \quad (14)$$

Preprints (www.preprints.org) | NOT PEER-REVIEWED | Posted: 6 November 2020 doi:10.20944/preprints202011.0226.v1

$$i = \frac{E}{D+E} \cdot k_e + \frac{D}{D+E} \cdot k_d \cdot (1-t), \quad (15)$$

$$f_{RM} = \frac{Maintenance + Salaries}{PI}, \quad (16)$$

where E and D are the amounts of equity and debt, k_e is the rate of return, k_d is the cost of debt, and t represents income taxes. The costs of maintenance stand at 8% of the equipment spent, and 2 workers per shift were considered necessary to keep the plant running, with individual annual salary costs estimated at € 40,000.

Finally, to define the vector and solve the economic balance, the annualized fixed costs flow is divided proportionally between the m subsystems of the plant:

$$FC_j = FC_A \cdot \frac{C_j}{C}. \quad (17)$$

3. Results and discussion

3.1. Energy and exergy cost analysis

The designed plant was analyzed at three different production scales, based on standard reactor capacities for hydrothermal carbonization [54]: 0.5 ton/h, 1 ton/h, and 2.5 ton/h of pruning wood for activated carbon. Additional mass flows of 1 ton/h, 2.1 ton/h, and 5.2 ton/h of winemaking waste were burned, respectively, to supply the energy process demands.

To complete the energy analysis, the size of the cogeneration cycle, as well as electric and heat equipment consumptions were estimated. Table 2 summarizes the overall electric and heat demand and other parameters considered in the analysis, while Fig. 3 shows main energy consumptions broken down by equipment and operation. To describe the process thoroughly, Fig. 4 notes the exergy flow balances of the plant designed to carbonize 500 kg/h of pruning wood.

Table 2. Energy demands of the plant and thermodynamic parameters considered for the exergetic analysis.

	0.5 ton/h	1 ton/h	2.5 ton/h
Electric consumption	297 kW	594 kW	1,485 kW
Heat supplied (burner)	3.70 MW	7.40 MW	18.50 MW
	Common parameters for energy analysis		
Burner exhaust gas temperature	1,473 K		
Inlet water temperature	286 K		
Thermal oil specific heat	2.54 $kJkg^{-1}K^{-1}$ [60]		
Ambient conditions	298 K, 1 atm		

Preprints (www.preprints.org) | NOT PEER-REVIEWED | Posted: 6 November 2020 doi:10.20944/preprints202011.0226.v1

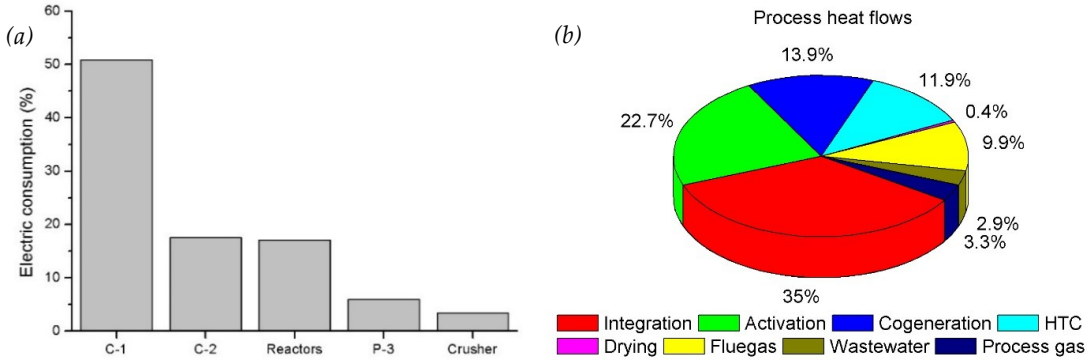

Figure 3. Relative equipment electric consumption (a) and heat flows distribution (b).

Compressor C-1, which compresses the air used to burn the wood and provide heat demands, comprises half of the total electricity consumption. Looking at the rest of equipment, the main consumers of electricity are the nitrogen compressor (C-2), the HTC reactor stirrers, the HTC reactor feeding pump (P-3), and the crusher. The remaining equipment represent minor electric consumptions, adding together to 5.2% of the overall.

The energy savings achieved by energy integration between hot and cold streams throughout the plant in heat exchangers E-1, E-2, E-3, E-4, and E-7 are remarkable, covering more than a third of the entire heat demand. The other 65% was provided by pruning wood combustion. Activation of hydrochar uses most of this heat. Thus, vaporization and heating up to 900 ºC in heat exchangers E-5 and E-6, and the endothermic character of the activation, hoard 22.7% of the plant heat flows.

Meanwhile, the heating of stream 11 up to 250 ºC in the hydrothermal carbonization reactors uses 11.9% and the drying of the hydrochar just 0.4%. Finally, the attached cogeneration cycle recovers more than half of the sensible heat of the outgoing flue gas and converts it into electricity, such that only 16.1% of the heat is lost in exiting exhaust gases, wastewater, and reaction waste gas.

a)

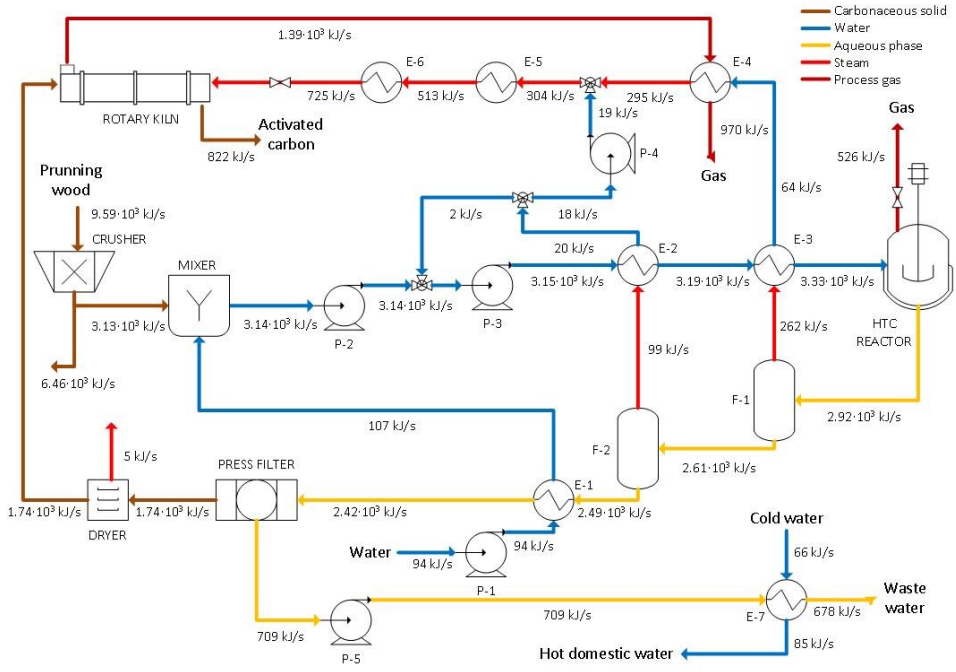

(b)

Preprints (www.preprints.org) | NOT PEER-REVIEWED | Posted: 6 November 2020 doi:10.20944/preprints202011.0226.v1

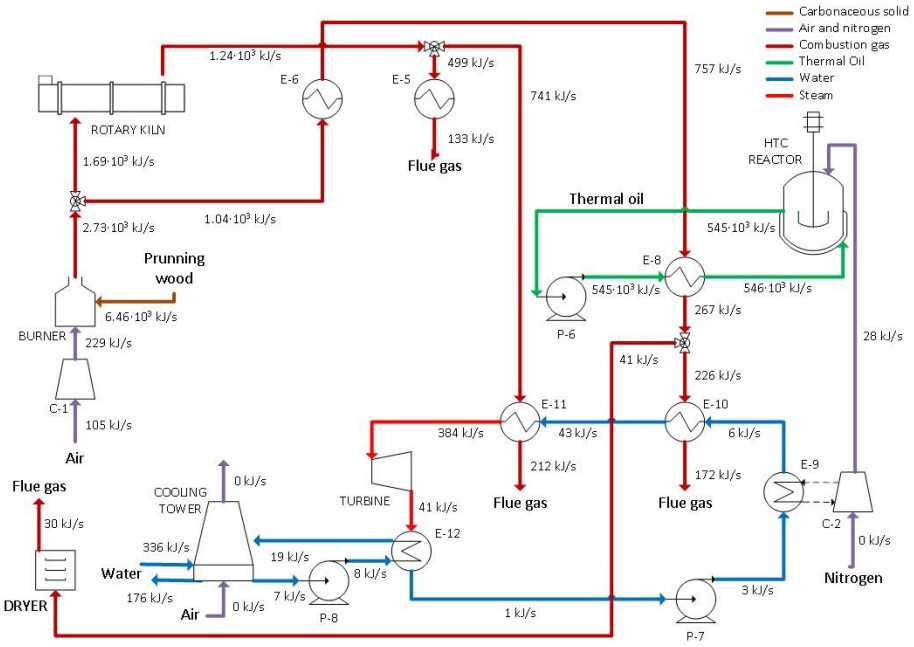

Figure 4. Exergy flows for a 500 kg/h pruning wood carbonization plant.

Fig. 5 shows the exergy cost analysis. The process has a cost of 12.27 exergy units for each exergy unit of activated carbon produced. In this calculation, chemical and physical exergies of substances and energy equipment demands are taken into account. On the other hand, the integrated Rankine cycle recovers one exergy unit for each 3.26 units contained in flue gas streams.

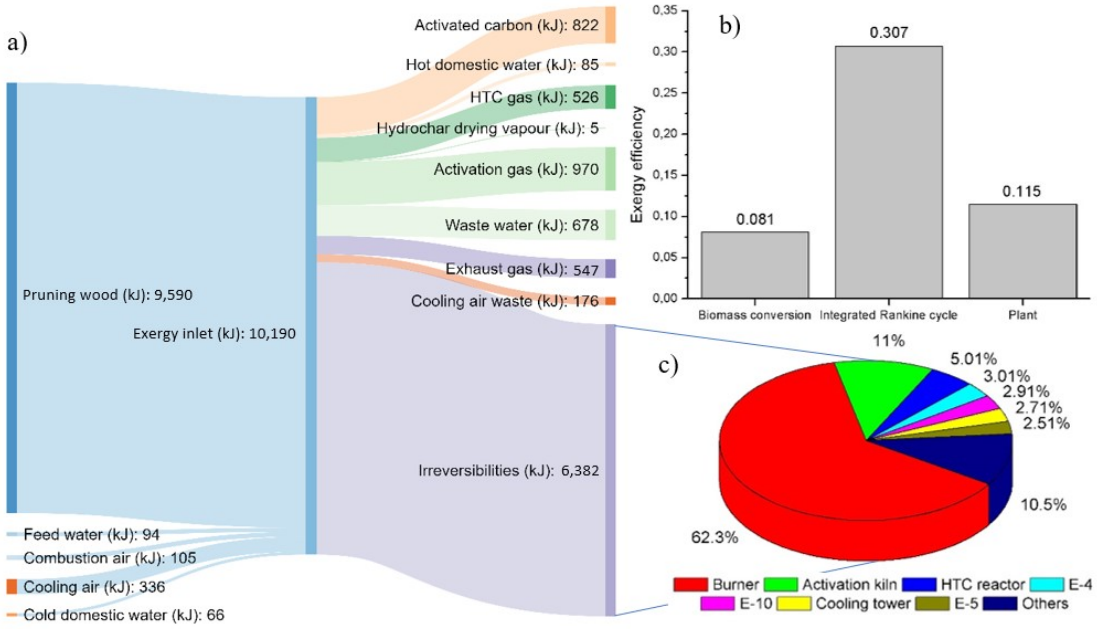

Figure 5. Sankey diagram of a 500 kg/h pruning wood carbonization plant (a); exergy efficiency of conversion, electric generation, and overall efficiency of the plant (b); and distribution of exergy destructions among the equipment of the plant (c).

As shown in Sankey diagram of Fig. 5a, more significant exergy losses happen due to chemical transformations, while thermodynamic equipment irreversibilities and heat loss represent minor

Preprints (www.preprints.org) | NOT PEER-REVIEWED | Posted: 6 November 2020 doi:10.20944/preprints202011.0226.v1

percentages. Considering activated carbon, electricity, and hot domestic water as products, the overall exergy costs of the plant descend to 8.72 units per exergy unit produced, corresponding to an exergy efficiency of 11.5% (Fig. 5b). In this way, the combustion of pruning wood in the burner causes a major destruction of exergy, followed by activation and hydrothermal carbonization (Fig. 5c). These results emphasize the importance of the energy integration achieved by the heat exchangers network.

3.2. Economic analysis

Economic investments into equipment, the plant, and process operations were estimated according to the procedure described in chapter 2.4.4 and noted in Table 3, with other economic parameters used as reference.

Costs of equity and debt give a cost of capital of 6.25%. These values are based on a financial analysis of chemical industry [61] and financial reports of the EU [55]; the profit tax rate was set at 25%, according to the current Spanish taxation. Operation of the plant was estimated as 15 years with 4 shifts of 2,000 hours each and 8,000 annual working hours. Pruning wood cost was estimated through an actualization of the prices of this kind of biomass; process water and wastewater costs through the public tariffs of a local water company; and electricity cost according to the Eurostat statistics for Spanish industrial consumers [56].

Figs. 6 and 7 show the influence of production scales on economic costs. The increase of scale is crucial to ensure the viability of the plant. At the smaller scale, the investments and fixed costs associated with the Rankine cycle have an excessive weight and make the plant unprofitable under market scenarios with electricity costs below 0.115 €/kWh. For the higher scales of 1 ton/h and 2.5 ton/h, the incorporation of the cogeneration cycle leads to adequate results (Fig. 6a). In contrast, the cost of hot domestic water supply does not differ significantly, being only affected by the price of mains water and the expenses relating to heat exchanger E-7 (Fig. 6b).

As expected, the increase of the scale notably reduced the weight of the fixed costs on total economic spending (Fig. 7a). Wood price stood out among the variable costs, supposing more than 30% of total investments during the plant service life. This is an important aspect in the economic analysis, as long as the wood used comes from winemaking waste and its price could be cut down easily [32], [57]. Fig. 7b compares the impact of the most expensive equipment on the fixed costs. Hydrothermal carbonization reactors accumulate the highest expenses. This result agrees with other economic analyses carried out for hydrochar production from hydrothermal carbonization of biomass [32],[34,35]. The relatively high spending dedicated to acquiring the batches and the nitrogen compressor indicates that the development of new semi-continuous or continuous industrial reactors might be a point of consideration to increase the competitivity of carbon product synthesis from biomass and wastes.

Table 3. Economic parameters considered for the economic analysis.

	500 kg/h	**1000 kg/h**	**2500 kg/h**
Investment on equipment (M€)	2.91	4.06	7.50
Working capital (M€)	2.18	3.05	5.63
Installation and start up (M€)	7.51	10.49	19.36
Annual maintenance (M€)	0.23	0.33	0.60
	Common parameters for economic analysis		
Annual salaries (M€)	0.32		
Debt to equity ratio	1.5		
Cost of equity / Cost of debt	0.1 / 0.05		
Taxes	25%		
Service life (years)	15		
Operation hours	8000		
Cost of pruning wood (€/ton)	73		

Preprints (www.preprints.org) | NOT PEER-REVIEWED | Posted: 6 November 2020 doi:10.20944/preprints202011.0226.v1

Cost of process water / cooling water (€/m³)	1.49 / 0.15
Cost of wastewater treatment (€/m³)	0.54
Cost of electricity (€/kWh)	0.11
€/$ exchange rate	1.10

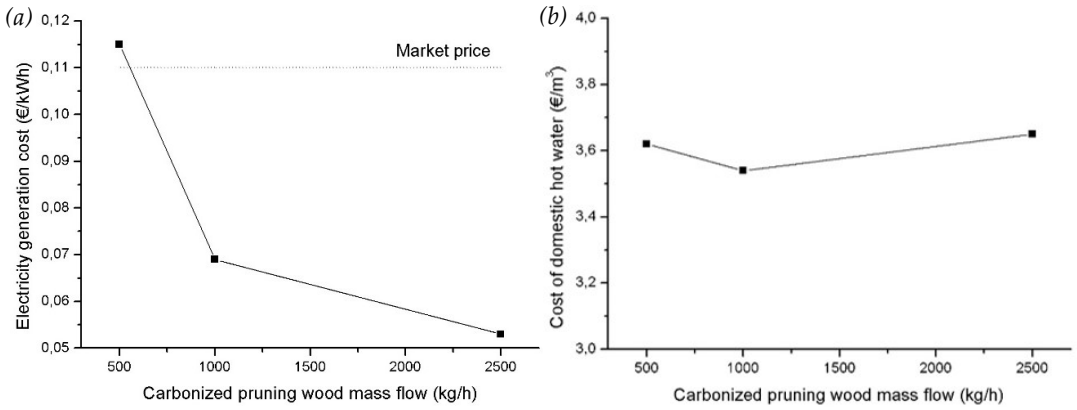

Figure 6. Costs of electricity (a) and costs of hot domestic water (b).

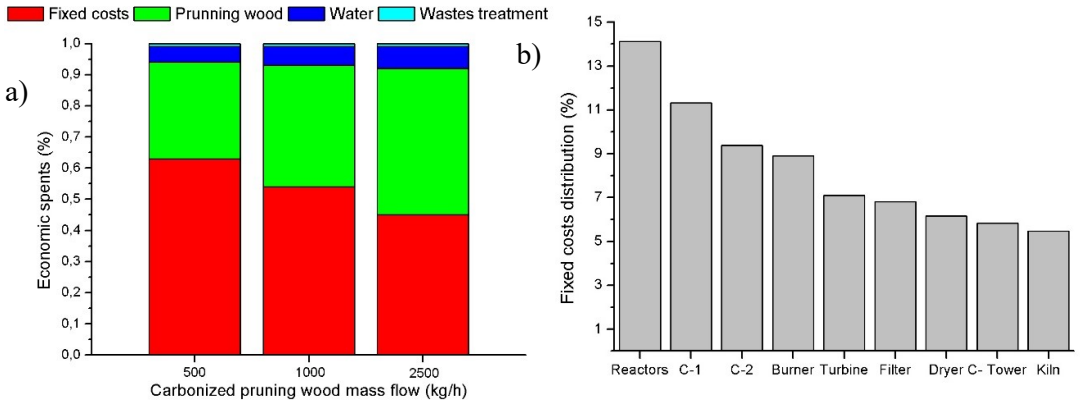

Figure 7. Economic investments distribution (a) and fixed cost distribution among the equipment (b).

3.3. Sensitivity analysis

A sensitivity analysis was carried out to determine the influence of economic and operational parameters on plant profitability. Figs. 8 and 9 show the activated carbon production costs variation with annual working hours, service life, cost of capital, and cost of pruning wood. To determine adequate economic scenarios, production costs of activated carbon obtained from wood (2.0 €/kg) and fossil carbon (1.10 €/kg) were set as targets [57,58].

The scale of production was demonstrated to be a fundamental parameter in economic plant viability and only at the highest scale was the plant systematically capable of achieving production costs which were competitive with wood activated carbon prices. Shifts and annual working hours also impacted the plant profitability significantly. Fig. 9a shows that it would be reasonable to

Preprints (www.preprints.org) | NOT PEER-REVIEWED | Posted: 6 November 2020 doi:10.20944/preprints202011.0226.v1

reduce the original 8,000 working hours to 6,000 working hours for the highest production scale. Further reductions on operational time could limit the economic feasibility, if other parameters were not improved. In this way, the cogeneration system clearly favors the plant competitivity under scenarios with higher workloads and service life.

Capital costs influenced the activated carbon prices moderately. Its increase caused a growth in plant investments, which marked an adverse tendency against the economic profits given by electricity cogeneration. In any case, the advantage of this system at high production scales is obvious and, even under other adverse scenarios, it manages to keep the production costs low, compared with one that takes the electricity from the grid.

Finally, pruning wood cost is the other great impact economic parameter, which is often the point of focus of projects working with wastes and low-cost raw materials. If the pruning wood cost stands at biomass market prices, the plant only would be able to compete with other biomass activated carbon process, but it is important to note that the wood used in the present research is a waste discarded by the wine industry and does not have any use as a consumer good. Besides, the accumulation of these residues can cause phytosanitary troubles and fires.

Legal regulation forces their proper treatment and elimination, such that its price may even be considered null if the plant is in a region with high winemaking activity. If the pruning wood procurement costs are under 15 € per ton, the obtained activated carbon would be competitive in price even with activated carbons made from coal, such that this process could open up a promising opportunity to replace activated carbons from fossil origin and help to change the industrial model in a new sustainable and ecological direction.

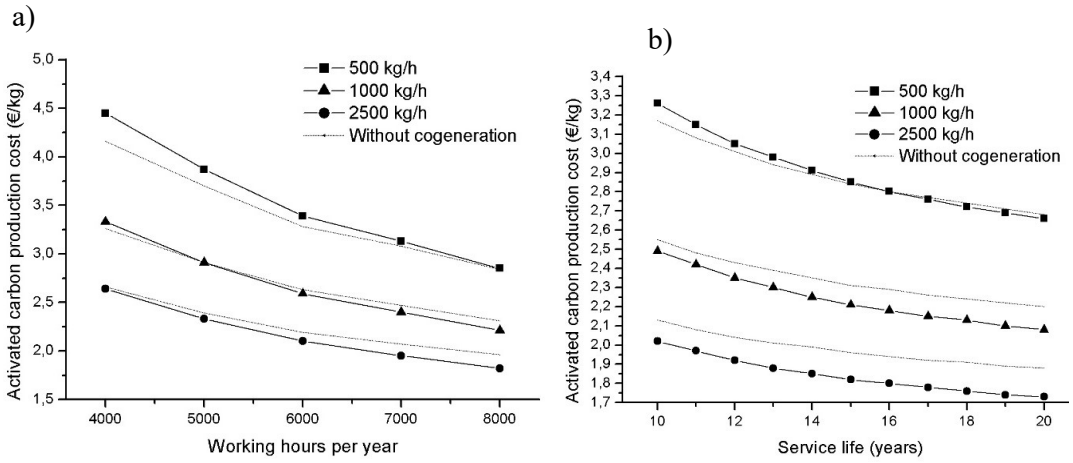

Figure 8. Activated carbon production costs variation in function of the working hours per year (a) and service life (b).

Preprints (www.preprints.org) | NOT PEER-REVIEWED | Posted: 6 November 2020 doi:10.20944/preprints202011.0226.v1

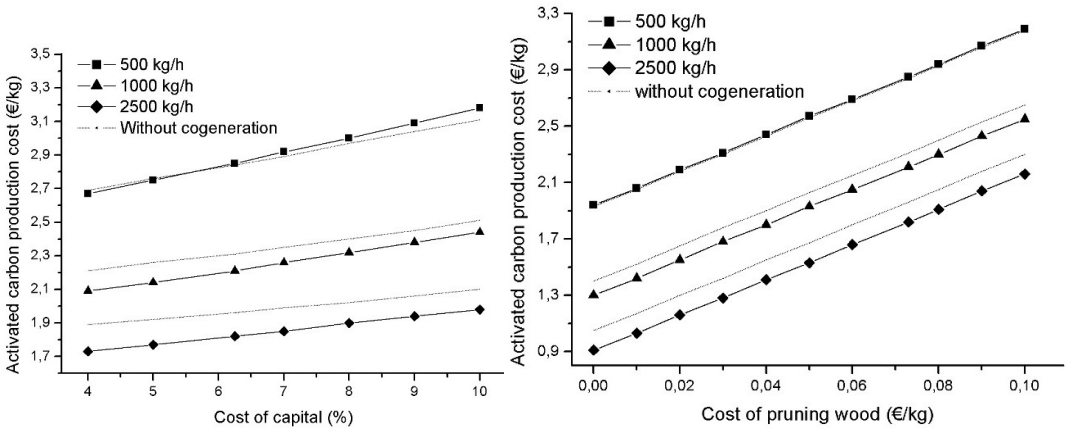

Figure 9. Activated carbon production costs variation in function of the cost of capital (a) and pruning wood (b).

4. Conclusions

Conversion of waste vineyard pruning wood into activated carbon was studied through experimental research to determine the products formed and the thermodynamics involved. The experimental results and thermoeconomic principles were used to design and model a sustainable production process for activated carbons using these wastes. The analysis focused on improving the efficiency of the plant through energy integration and the coupling of a cogeneration cycle which recovers the residual heat to provide the electric demands. Furthermore, economic and sensitivity analyses were performed to identify the competitive weakness of the plant and to consider the impacts of different parameters on its feasibility. According to the results, the following conclusions can be stated:

1. Pruning wood combustion used to supply heat demand causes the major destruction of exergy and, so, efficiency improvements should necessarily be focused on avoiding heat losses and reducing heat demands through recovery from remaining sources.

2. Energy integration and cogeneration are capable of covering 48.9% of the energy demands of the plant, which demonstrates the utility of the thermoeconomic method to identify the improvement opportunities in process efficiency.

3. High scales of production are fundamental to ensure the economic competitivity of the plant and to reduce the impact of the fixed costs on the overall balance.

4. At the highest scale of 2.5 ton/h of treated pruning wood, the plant achieves production costs which are competitive with activated carbon made from wood (2.0 €/kg). In this regard, the sensitivity analysis revealed the convenience of maintaining a workload above 6,000 working hours per year.

5. Pruning wood cost was the most important parameter in the economic sensitivity analysis. Obtaining reduced costs, due to its waste condition, could allow for ecological activated carbon generation which is competitive with bituminous products, which have production costs near 1.10 €/kg.

Nomenclature

Nomenclature
HTC: hydrothermal carbonization.
TOC: Total Organic Content.
GC-MS: gas chromatography-mass spectrometry.
HHV: higher heating value.
LHV: Lower Heating Value.
C_p: heat capacity.
u_{fsp}: fiber saturation point moisture.
P-1, P-2, P-3, P-4, P-5, P-6, P-7, P-8: pumps.
E-1, E-2, E-3, E-4, E-5, E-6, E-7, E-8, E-9, E-10, E-11, E-12: heat exchangers.
F-1, F-2: flash tanks.
C-1, C-2: compressors.
$A_{(m \times n)}$: incidence matrix.
B: stream exergy.
B_p: physical exergy.
B_c: chemical exergy.
B_d: destroyed exergy, thermodynamic irreversibilities.
$\dot{B}$: exergy flow.
T: temperature.
H, H^0: enthalpy and standard enthalpy of formation.
S, S_0: entropy and standard entropy of formation.
Z_H, Z_C, Z_O: mass fraction of hydrogen, carbon and oxygen.
B*: exergy cost.
$A^{-1}_{(n \times n)}$: inverse amplified incidence matrix.
$\Omega_{(n \times 1)}$: imputed exergy costs vector.
T: rational yield, exergy efficiency.
$\Pi_{(n \times 1)}$: thermoeconomic costs vector.
$\Phi_{(n \times 1)}$: imputed thermoeconomic costs vector.
FC_A: annualized fixed costs flow.
$A/P_{i,n}$: capital recovery factor.
f_{RM}: repair and maintenance factor.
PI: plant investment.
i: cost of capital.
n: plant lifetime.
E: equity.
D: debt.
k_e: cost of equity.
K_d: cost of debt.
t: income taxes.
FC: fixed costs flow.
C: cost of equipment.

References

1. European Commision An EU action plan for the circular economy. *Com* **2015**, *614*, 21, doi:10.1017/CBO9781107415324.004.
2. European Commision Report from the commision to the european parliament, the council, the european economic and social commitee and the committe of the regions on the

implementation of the Circular Economy Action Plan. *Com* **2019**, doi:10.1017/CBO9781107415324.004.

3. Dupuis, I. Producción y consumo sostenibles y residuos agrarios. *Minist. Agric. Aliment. y Medio Ambient.* **2012**, *66*, 37–39, doi:10.1007/s13398-014-0173-7.2.
4. Kambo, H. S.; Dutta, A. A comparative review of biochar and hydrochar in terms of production, physico-chemical properties and applications. *Renew. Sustain. Energy Rev.* **2015**, *45*, 359–378, doi:10.1016/j.rser.2015.01.050.
5. Brownsort, P.; Mašek, O. Biomass Pyrolysis Processes: Performance Parameters and their Influence on Biochar System Benefits. *SchoolofGeoSciences* **2009**, *MSc.*, 84.
6. López, F. A.; Centeno, T. A.; García-Díaz, I.; Alguacil, F. J. Textural and fuel characteristics of the chars produced by the pyrolysis of waste wood, and the properties of activated carbons prepared from them. *J. Anal. Appl. Pyrolysis* **2013**, *104*, 551–558, doi:10.1016/j.jaap.2013.05.014.
7. Haeldermans, T.; Campion, L.; Kuppens, T.; Vanreppelen, K.; Cuypers, A.; Schreurs, S. Bioresource Technology A comparative techno-economic assessment of biochar production from different residue streams using conventional and microwave pyrolysis. *Bioresour. Technol.* **2020**, *318*, 124083, doi:10.1016/j.biortech.2020.124083.
8. Rousset, P.; MacEdo, L.; Commandré, J. M.; Moreira, A. Biomass torrefaction under different oxygen concentrations and its effect on the composition of the solid by-product. *J. Anal. Appl. Pyrolysis* **2012**, *96*, 86–91, doi:10.1016/j.jaap.2012.03.009.
9. Puig-Arnavat, M.; Bruno, J. C.; Coronas, A. Review and analysis of biomass gasification models. *Renew. Sustain. Energy Rev.* **2010**, *14*, 2841–2851, doi:10.1016/j.rser.2010.07.030.
10. Brynda, J.; Skoblia, S.; Pohořelý, M.; Beňo, Z.; Soukup, K.; Jeremiáš, M.; Moško, J.; Zach, B.; Trakal, L.; Šyc, M. Wood chips gasification in a fixed-bed multi-stage gasifier for decentralized high-efficiency CHP and biochar production : Long-term commercial operation. *Fuel* **2020**, *281*, 118637, doi:10.1016/j.fuel.2020.118637.
11. Libra, J. A.; Ro, K. S.; Kammann, C.; Funke, A.; Berge, N. D.; Neubauer, Y.; Titirici, M. M.; Fühner, C.; Bens, O.; Kern, J.; Emmerich, K. H. Hydrothermal carbonization of biomass residuals: A comparative review of the chemistry, processes and applications of wet and dry pyrolysis. *Biofuels* **2011**, *2*, 71–106, doi:10.4155/bfs.10.81.
12. Reza, M. T.; Andert, J.; Wirth, B.; Busch, D.; Pielert, J.; Lynam, J. G.; Mumme, J. Hydrothermal Carbonization of Biomass for Energy and Crop Production. *Appl. Bioenergy* **2014**, *1*, 11–29, doi:10.2478/apbi-2014-0001.
13. Reza, M. T.; Uddin, M. H.; Lynam, J. G.; Hoekman, S. K.; Coronella, C. J. Hydrothermal carbonization of loblolly pine: reaction chemistry and water balance. *Biomass Convers. Biorefinery* **2014**, *4*, 311–321, doi:10.1007/s13399-014-0115-9.
14. Saba, A.; McGaughy, K.; Toufiq Reza, M. Techno-economic assessment of co-hydrothermal carbonization of a coal-Miscanthus blend. *Energies* **2019**, *12*, 1–17, doi:10.3390/en12040630.
15. Kruse, A.; Funke, A.; Titirici, M. M. Hydrothermal conversion of biomass to fuels and energetic materials. *Curr. Opin. Chem. Biol.* **2013**, *17*, 515–521, doi:10.1016/j.cbpa.2013.05.004.
16. Ramke, H.; Blöhse, D.; Lehmann, H.; Fettig, J. Hydrothermal Carbonization of Organic Waste. *Twelfth Int. Waste Manag. Landfill Symp.* **2009**.
17. Hoekman, S. K.; Broch, A.; Robbins, C. Hydrothermal carbonization (HTC) of lignocellulosic biomass. *Energy and Fuels* **2011**, *25*, 1802–1810, doi:10.1021/ef101745n.
18. Yan, W.; Hastings, J. T.; Acharjee, T. C.; Coronella, C. J.; Vásquez, V. R. Mass and energy

balances of wet torrefaction of lignocellulosic biomass. *Energy and Fuels* **2010**, *24*, 4738–4742, doi:10.1021/ef901273n.

19. Gamgoum, R.; Dutta, A.; Santos, R.; Chiang, Y. Hydrothermal Conversion of Neutral Sulfite Semi-Chemical Red Liquor into Hydrochar. *Energies* **2016**, *9*, 435, doi:10.3390/en9060435.
20. Alcaraz, L.; López Fernández, A.; García-Díaz, I.; López, F. A. Preparation and characterization of activated carbons from winemaking wastes and their adsorption of methylene blue. *Adsorpt. Sci. Technol.* **2018**, *36*, 1331–1351, doi:10.1177/0263617418770295.
21. Ramón-Gonçalves, M.; Alcaraz, L.; Pérez-Ferreras, S.; León-González, M. E.; Rosales-Conrado, N.; López, F. A. Extraction of polyphenols and synthesis of new activated carbon from spent coffee grounds. *Sci. Rep.* **2019**, *9*, 17706, doi:10.1038/s41598-019-54205-y.
22. Alcaraz, L.; Escudero, M. E.; Alguacil, F. J.; Llorente, I.; Urbieta, A.; Fernández, P.; López, F. A. Dysprosium Removal from Water Using Active Carbons Obtained from Spent Coffee Ground. *Nanomaterials* **2019**, *9*, 1372, doi:10.3390/nano9101372.
23. Björklund, K.; Li, L. Y. Adsorption of organic stormwater pollutants onto activated carbon from sewage sludge. *J. Environ. Manage.* **2017**, *197*, 490–497, doi:10.1016/j.jenvman.2017.04.011.
24. Jordá-Beneyto, M.; Suárez-García, F.; Lozano-Castelló, D.; Cazorla-Amorós, D.; Linares-Solano, A. Hydrogen storage on chemically activated carbons and carbon nanomaterials at high pressures. *Carbon N. Y.* **2007**, *45*, 293–303, doi:10.1016/j.carbon.2006.09.022.
25. Lim, J. Y.; Kang, D. A.; Kim, N. U.; Lee, J. M.; Kim, J. H. Bicontinuously crosslinked polymer electrolyte membranes with high ion conductivity and mechanical strength. *J. Memb. Sci.* **2019**, *589*, 117250, doi:10.1016/j.memsci.2019.117250.
26. Zhu, X.; Yu, S.; Xu, K.; Zhang, Y.; Zhang, L.; Lou, G.; Wu, Y.; Zhu, E.; Chen, H.; Shen, Z.; Bao, B.; Fu, S. Sustainable activated carbons from dead ginkgo leaves for supercapacitor electrode active materials. *Chem. Eng. Sci.* **2018**, *181*, 36–45, doi:10.1016/j.ces.2018.02.004.
27. Huwig, A.; Freimund, S.; Käppeli, O.; Dutler, H. Mycotoxin detoxication of animal feed by different adsorbents. *Toxicol. Lett.* **2001**, *122*, 179–188, doi:10.1016/S0378-4274(01)00360-5.
28. Gonzalez-Serrano, E.; Cordero, T.; Rodriguez-Mirasol, J.; Cotoruelo, L.; Rodriguez, J. J. Removal of water pollutants with activated carbons prepared from H 3PO4 activation of lignin from kraft black liquors. *Water Res.* **2004**, *38*, 3043–3050, doi:10.1016/j.watres.2004.04.048.
29. Zhang, T.; Walawender, W. P.; Fan, L. T.; Fan, M.; Daugaard, D.; Brown, R. C. Preparation of activated carbon from forest and agricultural residues through CO2 activation. *Chem. Eng. J.* **2004**, *105*, 53–59, doi:10.1016/j.cej.2004.06.011.
30. Nowicki, P.; Kazmierczak, J.; Pietrzak, R. Comparison of physicochemical and sorption properties of activated carbons prepared by physical and chemical activation of cherry stones. *Powder Technol.* **2014**, *269*, 312–319, doi:10.1016/j.powtec.2014.09.023.
31. Maciá-Agulló, J. A.; Moore, B. C.; Cazorla-Amorós, D.; Linares-Solano, A. Activation of coal tar pitch carbon fibres: Physical activation vs. chemical activation. *Carbon N. Y.* **2004**, *42*, 1367–1370, doi:10.1016/j.carbon.2004.01.013.
32. Lucian, M.; Fiori, L. Hydrothermal carbonization of waste biomass: Process design, modeling, energy efficiency and cost analysis. *Energies* **2017**, *10*, doi:10.3390/en10020211.
33. Stemann, J.; Erlach, B.; Ziegler, F. Hydrothermal carbonisation of empty palm oil fruit

bunches: Laboratory trials, plant simulation, carbon avoidance, and economic feasibility. *Waste and Biomass Valorization* **2013**, *4*, 441–454, doi:10.1007/s12649-012-9190-y.

34. Stemann, J.; Ziegler, F. Assessment of the Energetic Efficiency of A Continuously Operating Plant for Hydrothermal Carbonisation of Biomass. *World Renew. Energy Congr. 2011 - Sweden* **2011**, 125–132, doi:10.3384/ecp11057125.
35. Erlach, B.; Wirth, B.; Tsatsaronis, G. Co-Production of Electricity, Heat and Biocoal Pellets from Biomass: A Techno-Economic Comparison with Wood Pelletizing. *Proc. World Renew. Energy Congr. – Sweden, 8–13 May, 2011, Linköping, Sweden* **2011**, *57*, 508–515, doi:10.3384/ecp11057508.
36. Hitzl, M.; Corma, A.; Pomares, F.; Renz, M. The hydrothermal carbonization (HTC) plant as a decentral biorefinery for wet biomass. *Catal. Today* **2015**, *257*, 154–159, doi:10.1016/j.cattod.2014.09.024.
37. Valero, A.; Muñoz, M.; Lozano, M. A. General theory of exergy saving: II. On the thermoeconomic cost. In; Gaggioli, R., Ed.; 1986; Vol. 3, pp. 1–8.
38. Lozano, M. A.; Valero, A. Theory of the exergetic cost. *Energy* **1993**, *18*, 939–960, doi:10.1016/0360-5442(93)90006-Y.
39. Yang, K.; Zhu, N.; Ding, Y.; Chang, C.; Yuan, T. Thermoeconomic analysis of an integrated combined cooling heating and power system with biomass gasification. *Energy Convers. Manag.* **2018**, *171*, 671–682, doi:10.1016/j.enconman.2018.05.089.
40. Karellas, S.; Braimakis, K. Energy-exergy analysis and economic investigation of a cogeneration and trigeneration ORC-VCC hybrid system utilizing biomass fuel and solar power. *Energy Convers. Manag.* **2016**, *107*, 103–113, doi:10.1016/j.enconman.2015.06.080.
41. Mahmood, R.; Parshetti, G.; Balasubramanian, R. Energy, exergy and techno-economic analyses of hydrothermal oxidation of food waste to produce hydro-char and bio-oil. *Energy* **2016**, *102*, 187–198, doi:10.1016/j.energy.2016.02.042.
42. Linstrom, P. J.; Mallard, W. G. *NIST Chemistry WebBook, NIST Standard Reference Database Number 69*; National Institute of Standards and Technology: Gaithersburg MD, 20899;
43. Szargut, J. Appendix 1. Standard Chemical Exergy. *Thermodyn. Destr. Resour.* **2011**, 1–8, doi:https://doi.org/10.1017/CBO9780511976049.
44. Marsh, H.; Rodríguez-Reinoso, F. CHAPTER 5 - Activation Processes (Thermal or Physical). In *Activated Carbon*; Marsh, H., Rodríguez-Reinoso, F., Eds.; Elsevier Science Ltd: Oxford, 2006; pp. 243–321 ISBN 978-0-08-044463-5.
45. Ghouma, I.; Jeguirim, M.; Dorge, S.; Limousy, L.; Matei Ghimbeu, C.; Ouederni, A. Activated carbon prepared by physical activation of olive stones for the removal of NO2 at ambient temperature. *Comptes Rendus Chim.* **2015**, *18*, 63–74, doi:10.1016/j.crci.2014.05.006.
46. Funke, A.; Ziegler, F. Heat of reaction measurements for hydrothermal carbonization of biomass. *Bioresour. Technol.* **2011**, *102*, 7595–7598, doi:10.1016/j.biortech.2011.05.016.
47. Pecchi, M.; Patuzzi, F.; Benedetti, V.; Di Maggio, R.; Baratieri, M. Thermodynamics of hydrothermal carbonization: Assessment of the heat release profile and process enthalpy change. *Fuel Process. Technol.* **2020**, *197*, 106206, doi:10.1016/j.fuproc.2019.106206.
48. Radmanović, K.; Đukić, I.; Pervan, S. Specific Heat Capacity of Wood. *Drv. Ind.* **2014**, *65*, 151–157, doi:10.5552/drind.2014.1333.
49. Ptasinski, K. J. *Efficiency of Biomass Energy: An Exergy Approach to Biofuels, Power and Biorefineries*; John Wiley & Sons, 2016; ISBN 978-1-119-11816-9.

50. Seider, W. D.; Seader, J. D.; Lewin, D. R.; Wigado, S. *Product and Process Design Principles: Synthesis, Analysis and Evaluation*; 3rd ed.; Wiley, 2010;
51. U.S. Department of Energy Combined heat and power technology fact sheet series Available online: https://www.energy.gov/sites/prod/files/2016/09/f33/CHP-Steam Turbine.pdf. (accessed on 29/10(2020).
52. Norweigan University of Science and Technology Chemical Engineering Plant Cost Index (averaged over year). **2011**, 2020.
53. Peters, M. S.; Timmerhaus, M. D.; West, R. . *Plant Design and Economics for Chemical Engineers*; McGraw-Hill: New York, 2003;
54. De Dietrich PRODUCTS PORTFOLIO. Glass-lined Technology & other materials.
55. Gvetadze, S.; Kraemer-Eis, H.; Lang, F.; Prencipe, D.; Signore, S.; Torfs, W. EIF SME Access to Finance Index. *EIF Res. Mark. Anal.* **2018**.
56. Eurostat Electricity price statistics tables and graphs. **2019**, 1–12.
57. Akbari, M.; Oyedun, A. O.; Kumar, A. Techno-economic assessment of wet and dry torrefaction of biomass feedstock. *Energy* **2020**, *207*, 118287, doi:10.1016/j.energy.2020.118287.
58. Zanella, O.; Tessaro, I. C.; Féris, L. A. Desorption- and decomposition-based techniques for the regeneration of activated carbon. *Chem. Eng. Technol.* **2014**, *37*, 1447–1459, doi:10.1002/ceat.201300808.

Supplementary Materials: The following are available online at www.mdpi.com/xxx/s1, Figure S1. Solid yield of the HTC of vineyard pruning wood under experimental conditions (a) and elemental composition of raw and hydrochar after 1 hour of treatment (b); Figure S2. SEM image of the activated carbon porous structure obtained (a) and variation on the elemental composition during the activation treatment (b); Table S1. Mass balance of Hydrothermal Carbonization; Table S2. Non-condensable phase composition detected by GC-MS; Table S3. Elemental composition of the non-condensable organic phase analysed by GC-MS; Table S4. Chemical composition of the HTC aqueous phase assumed for the process analysis; Table S5. Chemical composition estimated for the HTC gaseous phase; Table S6. Mass balance of the activation; Table S7. Chemical composition estimated for the activation gas phase.

Author Contributions: Conceptualization, F.A.L. and F.J.A.; methodology, F.A.L., A.J.V. and F.J.A.; validation, I.L.; formal analysis, F.A.L. and I.L.; investigation, I.L.; resources, F.A.L.; data curation, I.L. and A.J.V.; writing—original draft preparation, I.L.; writing—review and editing, all authors.; supervision, F.A.L. and A.J.V.; Y.Y. All authors have read and agreed to the published version of the manuscript.

Funding: This research received no external funding

Acknowledgments: We acknowledge the support of the publication fee by the CSIC Open Access Publication Support Initiative through its Unit of Information Resources for Research (URICI

Conflicts of Interest: The authors declare no conflict of interest.